IEEE Access
Multidisciplinary | Rapid Review | Open Access Journal

Received January 17, 2020, accepted February 5, 2020, date of publication February 11, 2020, date of current version February 24, 2020.

Digital Object Identifier 10.1109/ACCESS.2020.2973295

Research on the Defected Ground Structure With von Koch Snowflake Fractals

XIN CAO, BOWEN LUO, YUYU ZHU, ZUXUE XIA, AND QIANGMING CAI
School of Information Engineering, Southwest University of Science and Technology, Mianyang 621010, China

Corresponding author: Xin Cao (caoxin@swust.edu.cn)

This work was supported by the Doctoral Foundation of Southwest University of Science and Technology under Grant 19zx7156.

ABSTRACT This paper studies the electromagnetic properties of defected ground structure (DGS) with von Koch snowflake fractals. First, the snowflake fractal is employed in the dumbbell shaped DGS, and we have discovered that it has the characteristics of a low-pass filter and the out-of-band rejection increases with fractal iterations. In consideration of fabrication accuracy and performance, the third iteration has been adopted. Based on this structure, we have designed a narrow-band filter and a wide-band filter to verify our theory. From the simulated and measured results, we can see that the out-of-band rejection level has been greatly improved. The proposed structure can be applied in communication planar circuits.

INDEX TERMS Bandpass filter, von Koch snowflake fractals, DGS, wide stopband.

I. INTRODUCTION

With the development of wireless communication technology, microwave devices with high performances are required. Filters are often used in these systems to extract useful signals, suppress unwanted interferences and reduce system noise [1]–[4]. Therefore, it is very important to improve out-of-band rejection of the planar filters achieve excellent system performance in modern communication circuits [5]–[9].

There are several ways that are commonly used in planar structures to increase the selectivity of the filter. One direct method is to cascade more resonators in the filter to steepen the slope of the transition band [10]–[14]. But using more resonators increases the size and in-band insertion loss. Also, it increases fabrication cost during mass production. Therefore, this method is sometimes used, but not recommended. Stepped impedance resonators (SIR) can also be employed to increase out-of-band rejection. By adjusting the impedance and electric length of each section, the harmonic passbands can be moved to a region that is farther away to the main passband [15]–[17]. This method requires high fabrication precision for the line width in the resonator can often be very thin [18], [19]. Defected ground structures (DGS) have been proposed during these decades. This structure is employed by etching periodic or non-periodic structure on the ground plane, so that the distributed capacitance and inductance of the transmission line are changed [20]–[24]. It can be regarded as an electromagnetic bandgap (EBG) structure and its equivalent circuit can be model as a parallel resonant circuit. If it is designed properly, transmission zeroes can be created in the transition band, thus increasing the out-of-band rejection.

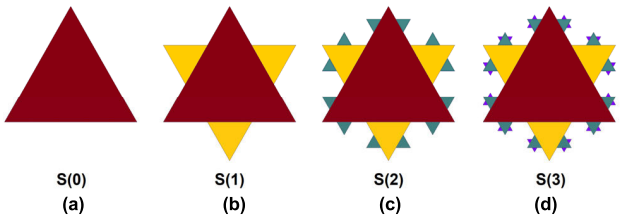

FIGURE 1. The island growing process of von Koch snowflake fractals (a) zeroth iteration (b) first iteration (c) second iteration (d) third iteration.

In the area of mathematics, fractals belong to a subset of Euclidean space that exhibit patterns with self-similarity. The topology replicates exactly itself at a smaller sale with infinity. Snowflake fractal was proposed by the Swedish mathematician Helge von Koch in 1904 [25]. It is created from a base triangle, from which sides grow smaller triangles, and so infinitum [26]. Figure 1 shows the topology of von Koch snowflake fractal at the zeroth, first, second and third iterations. We can see that several more triangles grow onto the original pattern after each iteration. The circumfluence can theoretically increase to infinity in a confined space.

The associate editor coordinating the review of this manuscript and approving it for publication was Haiwen Liu.

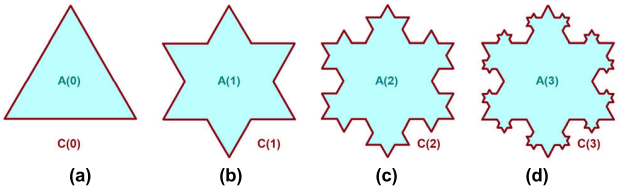

FIGURE 2. The island growing process of von Koch snowflake fractals (a) zeroth iteration (b) first iteration (c) second iteration (d) third iteration.

TABLE 1. The triangles and area added after each iteration.

Iteration	Area of one single triangle	number of added triangles	Total area added
0th	$A(0)$	1	$A(0)$
1st	$(1/9)A(0)$	3×4^{0}	$(3\times4^{0}\times1/9)A(0)$
2nd	$(1/9^{2})A(0)$	3×4^{1}	$(3\times4^{1}\times1/9^{2})A(0)$
3rd	$(1/9^{3})A(0)$	3×4^{2}	$(3\times4^{2}\times1/9^{3})A(0)$
n-th	$(1/9^{n})A(0)$	$3\times4^{n-1}$	$(3\times4^{n-1}\times1/9^{n})A(0)$

It looks like a paradox. But because of this property, we have discovered the potential applications in the microwave circuit.

In our design, we apply von Koch snowflake in the DGS structure and explore its electromagnetic properties. We also have designed two microwave planar filter with excellent performance. The filters are simulated and measured, and the results are in good agreement, which proves our proposed theory.

II. THEORY, ANALYSIS AND DESIGN PROCESS

The topology of the dumbbell DGS with a snowflake fractal of the third iteration is shown in figure 2. The yellow part is the signal line, which is on the top layer on the substrate. The red part is the metallic ground, which is on the bottom layer. The white part is the etched pattern. The snowflake fractal is on the one end of the long etched rectangle line. The fractal structure theoretically can achieve long circumference in a limited area, therefore it can effectively increase the distributed inductance, and can achieve low-pass filtering characteristics. Table 1 gives the triangles and area added after each iteration.

Let's suppose the area and circumference of $S(0)$ are $A(0)$ and $C(0)$. According to geometry, $A(n)$ can be calculated as

$$A(n) = A(0) + A(0)\sum_{k=1}^{n}\frac{4^{k-1}}{3^{2k-1}} = \frac{8}{5}A(0) - \frac{3}{5}\left(\frac{4}{9}\right)^{n}A(0) \quad (1)$$

Therefore,

$$\lim_{n\to+\infty} A(n) = \frac{8}{5}A(0) \quad (2)$$

Then, we can see the area of the snowflake fractal is 8/5 times the initial after an infinite number of iterations. The area is

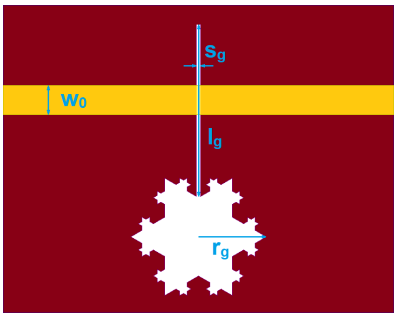

FIGURE 3. The topology of the DGS with a snowflake fractal of the third iteration.

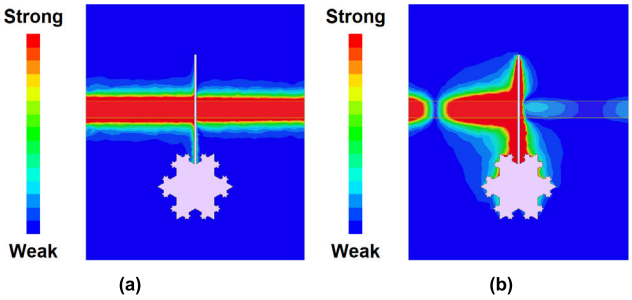

FIGURE 4. The electromagnetic field distribution at (a) passband and (b) stopband.

finite. $C(n)$ can also be calculated in a similar way as

$$C(n) = C(0) + C(0)\sum_{k=1}^{n}\frac{4^{k-1}}{3^{k}} = \left(\frac{4}{3}\right)^{n}C(n) \quad (3)$$

Therefore,

$$\lim_{n\to+\infty} C(n) = +\infty \quad (4)$$

The circumference of the snowflake fractal is infinite after an infinite number of iterations. Then we can see that if n approaches infinity, the circumference also reaches infinity while the area is a finite value. This property can show that the lowpass stopband can theoretically reach infinity if it is not limited by current PCB fabrication precision. To create parallel resonance, a slot line is connected to the fractal, and the topology is shown in figure 3.

Figure 4 gives the simulated electromagnetic field distribution at the passband and stopband. When the frequency is low, the electromagnetic wave travels through the snowflake fractal DGS with almost no reflection. With the increase of frequency, the electromagnetic wave is reflected and radiated by the snowflake fractal DGS, and a standing wave is formed on the input port of the line.

Considering the fabrication accuracy and our calculation, the maximum iteration used in our simulation is the third one. Figure 5 shows the simulated S_{21} of the snowflake DGS with the zeroth, first, second and third iterations. First, we can

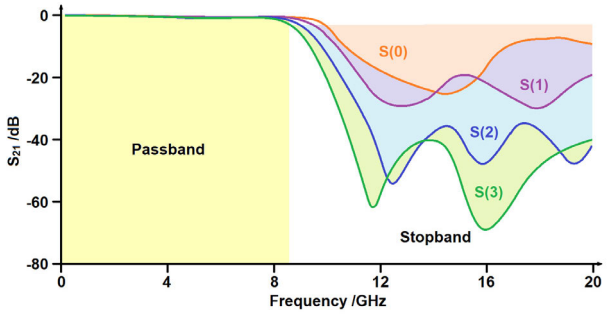

FIGURE 5. The simulated S_{21} of the snowflake DGS with the zeroth, first, second and third iterations.

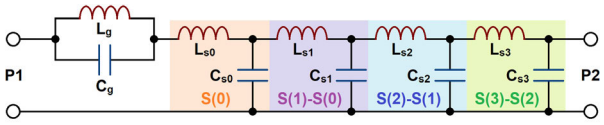

FIGURE 6. The equivalent circuit of the von Koch snowflake fractal DGS.

see that the out-of-band rejection level increases from around 20 dB at zeroth iteration to over 40 dB at the third iteration. The steepness of the slope also increases with iteration number. At the zeroth iteration, the slope is −6.6 dB/GHz, while at the third iteration, the slope is −13.5 dB/GHz.

The lowpass characteristics is due to the etched ground pattern, and its equivalent circuit model can be given in figure 6. L_g and C_g are created by the slot line on the ground, and they can be calculated as [27]

$$C_g = \frac{1}{g_1 Z_0 \omega_r \left(\frac{\omega_r}{\omega_c} - \frac{\omega_c}{\omega_r}\right)} \tag{5}$$

$$L_g = \frac{1}{\omega_r^2 C_g} \tag{6}$$

where g_1, ω_r, ω_c and Z_0 are the lowpass prototype value, resonant and cutoff angular frequencies of the transmission zero and characteristic impedance, respectively. The stage number increases with the increase of iteration number. For the snowflake fractal DGS, based on our simulation, the capacitance and inductance are mainly determined by the area and circumference, respectively. Then C_{sn} and L_{sn} can be estimated as

$$C_{sn} \simeq \frac{\varepsilon_r \left\{\frac{w_0}{d} + 0.667\left[2 + \ln\left(\frac{w_0}{d} + 1.444\right)\right]\right\}\left(e^{\varepsilon_r (A(n) - A(n-1))} - 1\right)}{120\pi v} \tag{7}$$

$$L_{sn} \simeq \frac{120\pi \mu_r}{v}\left\{\frac{e^{\mu_r (C(n) - C(n-1))} - 1}{\frac{w_0}{d} + 0.667\left[2 + \ln\left(w_0/d + 1.444\right)\right]}\right\} \tag{8}$$

where d is the thickness of the substrate; v is the guided wave velocity and t is the thickness of the ground plane.

In our design, quarter-wavelength resonators are employed as the resonant elements. This resonator has one open end and one shorted end. Therefore, at the resonant condition, the magnitude of voltage reaches the highest and the

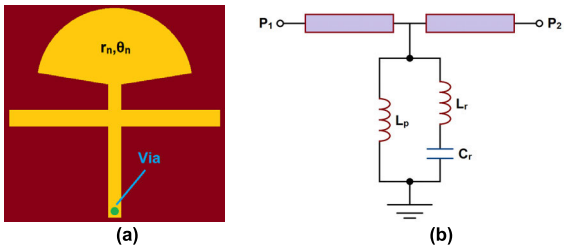

FIGURE 7. The topology (a) and equivalent circuit (b) of the quarter-wavelength resonator with one fan-shaped capacitor loaded at the open end.

magnitude of current reaches the lowest at the open end. At the shorted end, the magnitudes of voltage and current are opposite to those at open end. Then, the resonant wavelength is [28]

$$\lambda_r = \frac{\lambda_0}{2n+1} n \in N \tag{9}$$

where λ_0 is the longest resonant wavelength. Therefore, the resonant frequencies are

$$f_r = (2n+1) f_0 n \in N \tag{10}$$

Therefore, the first parasitic passband appears at $3f_0$. And in order to increase the selectivity of the designed filter, this passband should be suppressed. In our paper, periodic fan-shaped capacitors are utilized. Figure 7 shows the topology and equivalent circuit of the modified quarter-wavelength resonator with one fan-shaped capacitor loaded at the open end. L_r is the inductor of the line connected to the capacitor; C_r is the self-capacitance of the fan-shaped capacitor, and L_p is the inductance of the short-ended stub.

For fan-shaped capacitors, the capacitance and input impedance can be calculated as [29]

$$C_r = \frac{\theta_r r_0^2 \varepsilon_{eff}}{240\pi dc} \tag{11}$$

$$Z_{in} \cong -j\frac{120\pi d\beta}{\theta_r \sqrt{\varepsilon_{eff}}}\left(\frac{1}{2} + \frac{2}{(\beta r_0)^2}\right) \tag{12}$$

where ε_{eff}, d, c, β, θ_r, r_0 are the effective permittivity, substrate thickness, phase velocity of electromagnetic waves in vacuum, phase constant,fan angle and radius, respectively. For planar circuit, the effective permittivity can be given as [28]

$$\varepsilon_{eff} = \frac{\varepsilon_r + 1}{2} + \frac{\varepsilon_r - 1}{2} \cdot \frac{1}{\sqrt{1 + 12d/w}} \tag{13}$$

where w is the line width, and ε_r is the relative substrate permittivity. The equivalent circuit can generate one series resonance and one parallel resonance. The series resonant frequency f_z and parallel frequency f_0 can be calculated as

$$f_z = \frac{1}{2\pi\sqrt{L_r C_r}} \tag{14}$$

$$f_0 = \frac{1}{2\pi\sqrt{(L_p + L_r) C_r}} \tag{15}$$

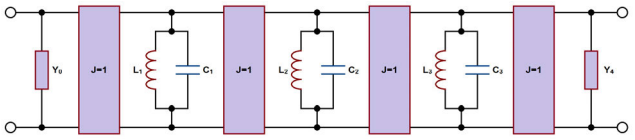

FIGURE 8. The general circuit model based on J-inverters.

The parallel resonant frequency f_0 creates the passband, while the series resonant frequency f_z creates one transmission zero in the network. If f_z is designed at $3f_0$, then the parasitic passband can be suppressed.

The connection lines between the resonators can be treated as J-inverters with the normalized admittance of unit. The general circuit model is shown in figure 8. Based on this circuit model, the center frequency f_0 is at the position where the admittance of the resonator is zero. The relative bandwidth can be controlled by the parallel stub of the resonator. Therefore, the component values L_i and C_i can be calculated based on the center frequency, relative bandwidth and element values in the low pass prototype, which is [30]

$$C_i = \frac{g_i}{RBW \cdot \omega_0 \cdot Z_0} \tag{16}$$

$$L_i = \frac{RBW \cdot Z_0}{\omega_0 \cdot g_i} \tag{17}$$

where g_i is the element values of the low pass prototype; RBW is the relative bandwidth of the passband and ω_0 is the center angular frequency.

Since there are three elements in the equivalent circuits, then it can be obtained from previous equations that

$$\frac{C_i}{C_r} = \frac{L_p + L_r}{L_i} \tag{18}$$

Therefore, all the component values can be calculated from g_i, RBW and f_0. The physical size of each section in the filter can be obtained from L_p, L_r and C_r. The length of the short-ended stub and capacitor connection line can be calculated as

$$l_p = \frac{L_p f_0 \lambda_0}{Z_p} \tag{19}$$

$$l_r = \frac{L_r f_0 \lambda_0}{Z_r} \tag{20}$$

where λ_0 is the guided wavelength of the electromagnetic wave at the center frequency. Z_p and Z_r are the impedance of the short-ended stub and capacitor connection line, respectively. The line width can be calculated using [28]

$$\frac{w}{d} = \begin{cases} \dfrac{8e^A}{e^{2A}-2} & w/d < 2 \\ \dfrac{2}{\pi}\left[B - 1 - \ln(2B-1)\right. & \\ \left. + \dfrac{\varepsilon_r - 1}{2\varepsilon_r}\left\{\ln(B-1) + 0.39 - \dfrac{0.61}{\varepsilon_r}\right\}\right] & w/d > 2 \end{cases} \tag{21}$$

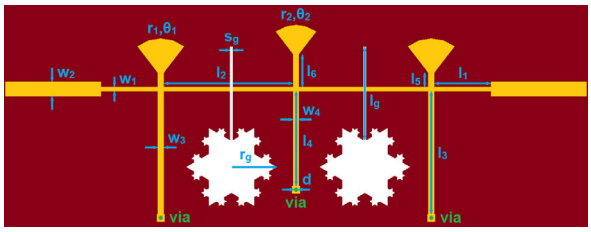

FIGURE 9. The topology of the proposed filter loaded with periodic fan-shaped capacitors.

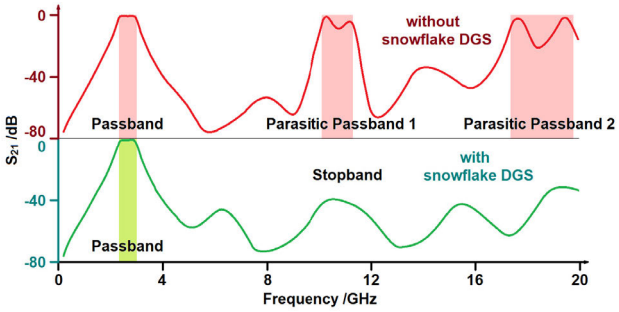

FIGURE 10. The topology of the proposed filter loaded with periodic fan-shaped capacitors.

where

$$A = \frac{Z}{60}\sqrt{\frac{\varepsilon_r + 1}{2}} + \frac{\varepsilon_r - 1}{\varepsilon_r + 1}\left(0.23 + \frac{0.11}{\varepsilon_r}\right) \tag{22}$$

$$B = \frac{377\pi}{2Z\sqrt{\varepsilon_r}} \tag{23}$$

The design specification requires the center frequency to be 3 GHz with relative bandwidth of 30%, therefore three stage Chebyshev response is chosen. The low pass element values are obtained as $g_1 = g_3 = 1.367$, $g_2 = 2.723$. Then the component values in the equivalent circuit can be calculated as $L_{p1} = L_{p3} = 1.33$ nH, $L_{p2} = 0.67$ nH, $C_{r1} = C_{r3} = 1.38$ pF, $C_{r2} = 2.75$ pF, $L_{r1} = L_{r3} = 0.71$ nH, $L_{r2} = 0.35$ nH. Therefore, the first resonator and the third one are of the same size, as shown in figure 9. The initial size of each section can be calculated using the component values based on the relative permittivity, loss tangent and thickness of the substrate.

Figure 10 gives the simulated results with and without the snowflake fractal DGS. We can see that the second and third harmonic passbands have been suppressed greatly. Also, the out-of-band rejection is over 35 dB in the stopband.

The substrate used in the design is Rogers 5880 with the relative permittivity $\varepsilon_r = 2.2$, loss tangent $\tan\delta = 0.0009$, and thickness $h = 0.508$ mm. The filter is simulated using HFSS and the photograph of the proposed filter is shown in figure 11. After optimization, the physical size of each section can be given as (length in mm): $w_1 = 0.5$, $w_2 = 1.5$, $w_3 = 0.6$, $w_4 = 0.6$, $l_1 = 6.0$, $l_2 = 13.6$, $l_3 = 13.0$, $l_4 = 10.0$, $l_5 = 1.5$, $l_6 = 3.4$, $r_1 = 4.0$, $r_2 = 3.5$, $d = 0.5$, and $r_g = 4.7$.

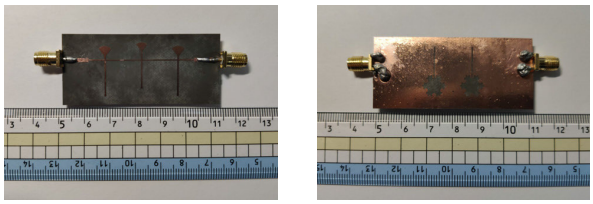

FIGURE 11. The photograph of the proposed filter (a) top view (b) bottom view.

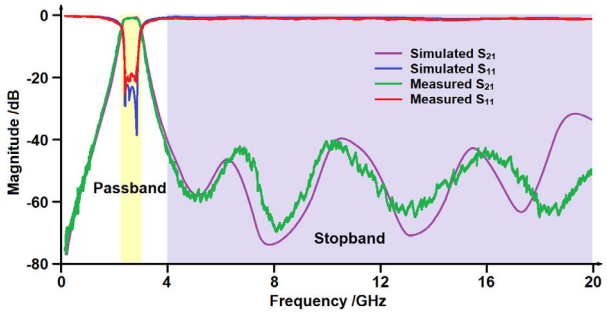

FIGURE 12. The simulated and measured results of the proposed filter.

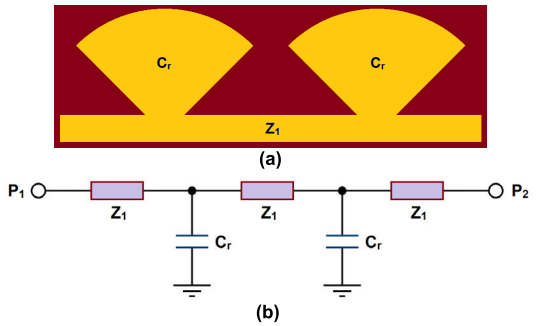

FIGURE 13. The topology (a) and equivalent circuit (b) of the transverse line loaded with periodic fan-shaped capacitors.

The simulated and measured results are shown in figure 12. The filter is measured using Keysight PNA-X network analyzer N5247B. The measured center frequency is 3.0 GHz with the relative bandwidth of 29%. The in-band insertion loss is less than 1.0 dB and the return loss better than 19 dB. The suppression of the parasitic passband at the third harmonic is over 40 dB. The simulated and measured results are in good agreement and the selectivity of the filter has been improved.

Also the proposed structure can be employed in the wideband band-pass filters to improve out-of-band rejection. Figure 13 shows the topology and equivalent circuit of the transverse line loaded with periodic fan-shaped capacitors.

Therefore, the low-pass cutoff frequency can be calculated as

$$f_B = \frac{1}{\pi\sqrt{L\,(C + C_r)}} \tag{24}$$

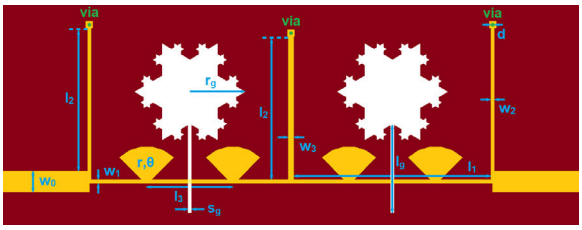

FIGURE 14. The topology of the proposed filter.

where L and C are the distributed inductance and capacitance respectively. C_r is the capacitance of the fan-shaped capacitor. The characteristic impedances of the loaded line and unloaded line can be denoted as

$$Z_L = \sqrt{\frac{L}{C + C_r}} \tag{25}$$

$$Z_1 = \sqrt{\frac{L}{C}} \tag{26}$$

And the phase shift of the loaded line can be given as

$$\varphi = 2\pi f\sqrt{L\,(C + C_r)} \tag{27}$$

When the design specifications are given, L, C and C_r are unknown variables.

In order for the stopband range to exceed over 20 GHz, and also based on the cutoff frequency of the stopband, the characteristic impedance of the line is calculated to be 50 Ω with the phase shift of 45°, then L, C and C_r can be denoted based on the impedance, phase shift and cutoff frequency of the unit cell. The formulas can be derived as

$$L = \frac{Z_L\varphi}{2\pi f_0} \tag{28}$$

$$C = \frac{Z_L\varphi}{2\pi f_0 Z_1^2} \tag{29}$$

$$C_r = \frac{L}{Z_L^2} - C \tag{30}$$

C, L and C_r in our case can be calculated to be 0.18 pF, 3.5 nH and 1.4 pF, respectively. Therefore, Z_1 and f_B can be calculated to be 125 Ω and 6.3 GHz.

In our design, three segments of short-ended lines are employed as the resonant units, and they produce the passband of the filter. The width of the center transverse line is thinner to create high impedance. Two fan-shaped capacitors are added between every two resonators to suppress harmonic passbands. The topology of the proposed filter is shown in figure 14.

Figure 15 shows the simulated S_{21} of the filters with or without the fan-shaped capacitors. The width and length of these two filters are modified due to the changes in distributed capacitance and inductance after loading the fan-shaped capacitors. It can be seen that the original filter without the capacitors have parasitic passbands at the third and fifth harmonics. After loading the capacitors, the harmonics have been suppressed without affecting the performance of the

TABLE 2. Table of performance comparison.

Ref.	f_0 (GHz)	IB-IL (dB)	IB-RL (dB)	RBW (%)	IL@$2f_0$ (dB)	IL@$3f_0$ (dB)	IL@$4f_0$ (dB)	IL@$5f_0$ (dB)	IL@$6f_0$ (dB)	Maximum Rejection (dB)
[31]	9.0	2.3	10	33	45	-	-	-	-	50
[32]	4.0	1.4	14	45	25	-	-	-	-	53
[33]	6.8	1	17	110	23	34	35	-	-	50
[34]	1.6	2.2	14	5	39	32	8	22	-	81
[35]	1.0	1.6	10	123	33	57	40	32	8	59
[36]	2.0	1.1	12	115	50	69	59	42	47	79
filter 1	3.0	1.0	19	29	45	61	55	43	58	68
filter 2	3.4	1.2	18	143	58	63	67	62	46	73

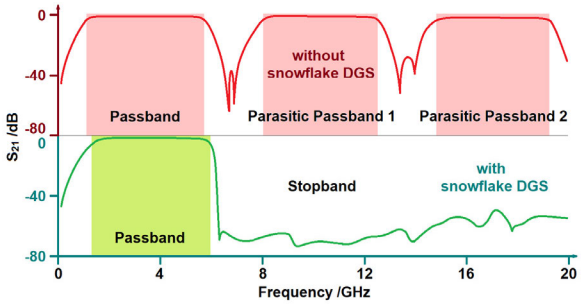

FIGURE 15. The simulated S_{21} of the filters with or without snowflake DGS.

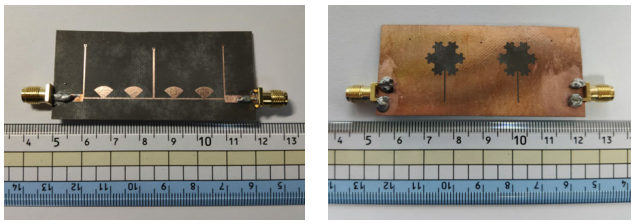

FIGURE 16. The photograph of the proposed filter (a) top view (b) bottom view.

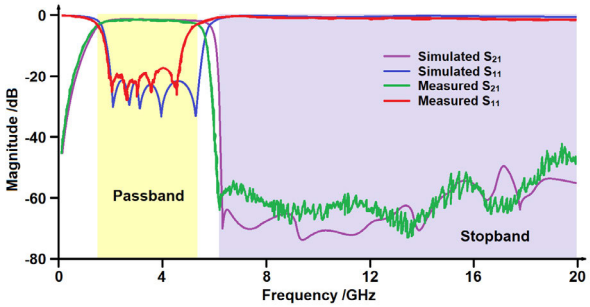

FIGURE 17. The simulated and measured S-parameters of the proposed filter.

passband. From 8 GHz to 20 GHz, the rejection level is over 40 dB and the selectivity of the filter has been greatly improved.

Figure 16 shows the photograph of the proposed filter. The Rogers 5880 substrate is employed, with the relative permittivity $\varepsilon_r = 2.2$, dissipation factor, tan $\delta = 0.0009$ and thickness $h = 0.787$ mm. The geometric parameters are given as (length in mm): $w_0 = 2.4$, $w_1 = 0.4$, $w_2 = 0.4$, $w_3 = 0.6$, $w_4 = 0.8$, $l_1 = 23.4$, $l_2 = 16.9$, $l_3 = 10.3$, $r = 4.4$, $d = 0.5$, and $r_g = 6.9$.

Figure 17 shows the simulated and measured S_{21} of the proposed filter. From the measured results, the selectivity of the filter has been improved. From 6 GHz to 20 GHz, the out-of-band rejection is higher than 40 dB. The center frequency of the passband is 3.4 GHz, with the relative bandwidth of 143%. The in-band insertion loss is lower than 1.2 dB, and the return loss is better than 18 dB. The measured results are in good agreement with the simulated results.

Performances comparison of some other filters in terms of center frequency (f_0), in-band insertion loss (IB-IL), in-band return loss (IB-RL), relative bandwidth (RBW), insertion loss from the second to sixth harmonics, and maximum out-of-band rejection in the references are listed in table 2. It can be seen that comparable performances have been achieved.

III. CONCLUSION

In this paper, we have investigated and analyzed the electromagnetic property of the DGS with von Koch fractals and its potential applications in microwave planar filters. The fractal structure theoretically has an infinite rejection band if it is not limited by current precision level of PCB fabrication technology. Two band-pass filters have been designed based on the proposed structure and wide out-of-band rejection has been achieved. The proposed structure can be applied in modern planar circuits to improve performance.

APPENDIX

The fractal curve can be created using rotation matrices with building matrices. For each iteration, the fractal line is generated on the islands of the last iteration. For von Koch snowflake fractals, building functions are given as

$$g_0(x) = \begin{bmatrix} 1/3 & 0 \\ 0 & 1/3 \end{bmatrix} r + \begin{bmatrix} 1/3 \\ \sqrt{3}/3 \end{bmatrix} \quad \text{(a1)}$$

$$g_{1+}(x) = \begin{bmatrix} 1/2 & -\sqrt{3}/6 \\ \sqrt{3}/6 & 1/2 \end{bmatrix} r + \begin{bmatrix} 1/3 \\ 0 \end{bmatrix} \quad \text{(a2)}$$

$$g_{1-}(x) = \begin{bmatrix} -1/6 & \sqrt{3}/6 \\ -\sqrt{3}/6 & -1/6 \end{bmatrix} r + \begin{bmatrix} 1/6 \\ \sqrt{3}/6 \end{bmatrix} \quad \text{(a3)}$$

$$g_{2+}(x) = \begin{bmatrix} 1/6 & -\sqrt{3}/6 \\ \sqrt{3}/6 & 1/6 \end{bmatrix} r + \begin{bmatrix} 1/6 \\ \sqrt{3}/6 \end{bmatrix} \quad \text{(a4)}$$

$$g_{2-}(x) = \begin{bmatrix} 1/6 & \sqrt{3}/6 \\ -\sqrt{3}/6 & 1/6 \end{bmatrix} r + \begin{bmatrix} 2/3 \\ \sqrt{3}/6 \end{bmatrix} \quad \text{(a5)}$$

$$g_{3+}(x) = \begin{bmatrix} -1/3 & 0 \\ 0 & -1/3 \end{bmatrix} r + \begin{bmatrix} 2/3 \\ 0 \end{bmatrix} \quad \text{(a6)}$$

$$g_{3-}(x) = \begin{bmatrix} 1/3 & 0 \\ 0 & 1/3 \end{bmatrix} r + \begin{bmatrix} 2/3 \\ 0 \end{bmatrix} \quad \text{(a7)}$$

REFERENCES

[1] D. Lu, M. Yu, N. S. Barker, Z. Li, W. Li, and X. Tang, "Advanced synthesis of wide-tuning-range frequency-adaptive bandpass filter with constant absolute bandwidth," *IEEE Trans. Microw. Theory Techn.*, vol. 67, no. 11, pp. 4362–4375, Nov. 2019.

[2] M. D. Hickle and D. Peroulis, "Tunable constant-bandwidth substrate-integrated bandstop filters," *IEEE Trans. Microw. Theory Techn.*, vol. 66, no. 1, pp. 157–169, Jan. 2018.

[3] D. Psychogiou and R. Gomez-Garcia, "Multi-mode-cavity-resonator-based bandpass filters with multiple levels of transfer-function adaptivity," *IEEE Access*, vol. 7, pp. 24759–24765, 2019.

[4] Z. Shen, K. Xu, G. M. Mbongo, J. Shi, and Y. Yang, "Compact balanced substrate integrated waveguide filter with low insertion loss," *IEEE Access*, vol. 7, pp. 126111–126115, 2019.

[5] X. Cao, J. Bao, and Z. Tang, "Design of a dual-band waveguide filter based on micromachining fabrication process," *IET Microw., Antennas Propag.*, vol. 10, no. 4, pp. 459–463, Mar. 2016.

[6] R. Gomez-Garcia, R. Loeches-Sanchez, D. Psychogiou, and D. Peroulis, "Single/multi-band Wilkinson-type power dividers with embedded transversal filtering sections and application to channelized filters," *IEEE Trans. Circuits Syst. I, Reg. Papers*, vol. 62, no. 6, pp. 1518–1527, Jun. 2015.

[7] X. Cao, Z. X. Tang, and F. Wang, "A method of designing dual-band bandpass filter using the hexagon CRLH resonators and cascaded defected ground structure," *Microw. Opt. Technol. Lett.*, vol. 57, no. 8, pp. 1876–1879, Aug. 2015.

[8] S. Saeedi, J. Lee, and H. H. Sigmarsson, "Tunable, high-Q, substrate-integrated, evanescent-mode cavity bandpass-bandstop filter cascade," *IEEE Microw. Wireless Compon. Lett.*, vol. 26, no. 4, pp. 240–242, Apr. 2016.

[9] T. Saito, S. Kodama, T. Saito, S. Ohshima, and A. Saito, "Design of high power handling filter using cascaded quadruplet superconducting bulk resonators," *IEEE Trans. Appl. Supercond.*, vol. 28, no. 4, pp. 1–4, Jun. 2018.

[10] M. Esmaeili and J. Bornemann, "Substrate integrated waveguide triple-passband dual-stopband filter using six cascaded singlets," *IEEE Microw. Wireless Compon. Lett.*, vol. 24, no. 7, pp. 439–441, Jul. 2014.

[11] D. Psychogiou and R. Gomez-Garcia, "Reflectionless adaptive RF filters: Bandpass, bandstop, and cascade designs," *IEEE Trans. Microw. Theory Techn.*, vol. 65, no. 11, pp. 4593–4605, Nov. 2017.

[12] Z.-C. Hao and J.-S. Hong, "UWB bandpass filter using cascaded miniature high-pass and low-pass filters with multilayer liquid crystal polymer technology," *IEEE Trans. Microw. Theory Techn.*, vol. 58, no. 4, pp. 941–948, Apr. 2010.

[13] M. Yuceer, "A reconfigurable microwave combline filter," *IEEE Trans. Circuits Syst. II, Exp. Briefs*, vol. 63, no. 1, pp. 84–88, Jan. 2016.

[14] R. Gomez-Garcia, J.-M. Munoz-Ferreras, J. Jimenez-Campillo, F. Branca-Roncati, and P. Martin-Iglesias, "High-order planar bandpass filters with electronically-reconfigurable passband width and flatness based on adaptive multi-resonator cascades," *IEEE Access*, vol. 7, pp. 11010–11019, 2019.

[15] W. Qin, J. Cai, Y.-L. Li, and J.-X. Chen, "Wideband tunable bandpass filter using optimized varactor-loaded SIRs," *IEEE Microw. Wireless Compon. Lett.*, vol. 27, no. 9, pp. 812–814, Sep. 2017.

[16] X. Cao, Z. Tang, F. Wang, Y. Wu, W. Yao, B. Zhang, and Y. Wang, "A novel tri-band band-pass filter using combined simplified CRLH and right-handed SIRs," *J. Electromagn. Waves Appl.*, vol. 27, no. 8, pp. 999–1007, May 2013.

[17] R. Gomez-Garcia, L. Yang, J.-M. Munoz-Ferreras, and D. Psychogiou, "Selectivity-enhancement technique for stepped-impedance-resonator dual-passband filters," *IEEE Microw. Wireless Compon. Lett.*, vol. 29, no. 7, pp. 453–455, Jul. 2019.

[18] J. Shi, L. Lin, J.-X. Chen, H. Chu, and X. Wu, "Dual-band bandpass filter with wide stopband using one stepped-impedance ring resonator with shorted stubs," *IEEE Microw. Wireless Compon. Lett.*, vol. 24, no. 7, pp. 442–444, Jul. 2014.

[19] H. Liu, Y. Peng, B. Ren, P. Wen, J. Lei, and X. Guan, "Compact triple-band superconducting filter based on a multimode stepped-impedance split-ring resonator," *IEEE Trans. Appl. Supercond.*, vol. 26, no. 6, pp. 1–5, Sep. 2016.

[20] G. Chaudhary, H. Choi, Y. Jeong, J. Lim, D. Kim, and J.-C. Kim, "Design of dual-band bandpass filter using DGS with controllable second passband," *IEEE Microw. Wireless Compon. Lett.*, vol. 21, no. 11, pp. 589–591, Nov. 2011.

[21] B. Peng, S. Li, J. Zhu, Q. Zhang, L. Deng, Q. Zeng, and Y. Gao, "Compact quad-mode bandpass filter based on quad-mode DGS resonator," *IEEE Microw. Wireless Compon. Lett.*, vol. 26, no. 4, pp. 234–236, Apr. 2016.

[22] Y. Han, Z. Liu, C. Zhang, C. Mei, Q. Chen, K. Hu, and S. Yuan, "A flexible microstrip low-pass filter design using asymmetric pi-shaped DGS," *IEEE Access*, vol. 7, pp. 49999–50006, 2019.

[23] X. Cao, Z. Tang, F. Wang, and K. Yang, "A tunable dual-band bandpass filter using asymmetrical varactor-loaded HWRs and defected ground structure," *IEICE Electron. Express*, vol. 12, no. 13, 2015, Art. no. 20150482.

[24] F.-C. Chen, H.-T. Hu, J.-M. Qiu, and Q.-X. Chu, "High-selectivity low-pass filters with ultrawide stopband based on defected ground structures," *IEEE Trans. Compon., Packag., Manuf. Technol.*, vol. 5, no. 9, pp. 1313–1319, Sep. 2015.

[25] E. W. Dekking and F. M. Dekking, "Helge von Koch's snowflake curve revisited," *Amer. Math. Monthly*, vol. 123, no. 2, pp. 181–186, 2016.

[26] Y. D. Sergeyev, "The exact (up to infinitesimals) infinite perimeter of the Koch snowflake and its finite area," *Commun. Nonlinear Sci. Numer. Simul.*, vol. 31, nos. 1–3, pp. 21–29, Feb. 2016.

[27] D.-J. Jung and K. Chang, "Low-pass filter design through the accurate analysis of electromagnetic-bandgap geometry on the ground plane," *IEEE Trans. Microw. Theory Techn.*, vol. 57, no. 7, pp. 1798–1805, Jul. 2009.

[28] D. M. Pozar, *Microwave Engineering*, 4th ed. Hoboken, NJ, USA: Wiley, 2012.

[29] L. Zhu, S. Sun, and R. Li, *Microwave Bandpass Filters for Wideband Communications*. vol. 232. Hoboken, NJ, USA: Wiley, 2011.

[30] J.-S. G. Hong and M. J. Lancaster, *Microstrip Filters for RF/Microwave Applications*. vol. 167. Hoboken, NJ, USA: Wiley, 2004.

[31] L. Ye, Y. Chen, K. D. Xu, W. Li, Q. H. Liu, and Y. Zhang, "Substrate integrated plasmonic waveguide for microwave bandpass filter applications," *IEEE Access*, vol. 7, pp. 75957–75964, 2019.

[32] Z.-C. Zhang and H. Liu, "A ultra compact wideband bandpass filter using a quadmode stub-loaded resonator," *Prog. Electromagn. Res.*, vol. 77, pp. 35–40, 2018.

[33] Z. Sakotic, V. Crnojevic-Bengin, and N. Jankovic, "Compact circular-patch-based bandpass filter for ultra-wideband wireless communication systems," *AEU-Int. J. Electron. Commun.*, vol. 82, pp. 272–278, Dec. 2017.

[34] M. Mimsyad, C. G. Hsu, and M. Ho, "Ultra-miniaturization design of substrate-integrated waveguide cavity trisection bandpass filter," *Microw. Opt. Technol. Lett.*, vol. 61, no. 12, pp. 2826–2831, Dec. 2019.

[35] X. Gao, W. Feng, and W. Che, "Compact ultra-wideband bandpass filter with improved upper stopband using open/shorted stubs," *IEEE Microw. Wireless Compon. Lett.*, vol. 27, no. 2, pp. 123–125, Feb. 2017.

[36] Z. Li and K.-L. Wu, "Direct synthesis and design of wideband bandpass filter with composite series and shunt resonators," *IEEE Trans. Microw. Theory Techn.*, vol. 65, no. 10, pp. 3789–3800, Oct. 2017.

XIN CAO received the B.S., M.S., and Ph.D. degrees from the University of Science and Technology of China, in 2011, 2014, and 2018, respectively. He is currently with the Southwest University of Science and Technology. His current areas of interest include electromagnetics, microwave circuits, and applied mathematics.

BOWEN LUO was born in 1997. He received the bachelor's degree in communications engineering from the Southwest University of Science and Technology. He is currently pursuing the master's degree with the School of Information Engineering, Electronics and Communication Engineering. His main research areas are microwave circuits, electromagnetic compatibility technology, and 5G MIMO array antennas.

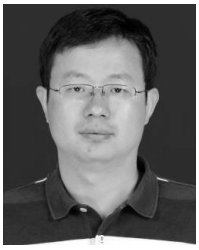

YUYU ZHU received the B.S. and M.S. degrees from the Southwest University of Science and Technology. He is currently pursuing the Ph.D. degree in non-destructive testing with the University of Electronic Science and Technology. He has long been involved in the research of power electronics applications and electromagnetic compatibility, non-destructive testing, and measurement, and control systems.

ZUXUE XIA received the Ph.D. degree in electromagnetic field and microwave from the University of Science and Technology of China. He has been involved in microwave passive components, especially microwave filter design, power divider, coupler design, and antenna design.

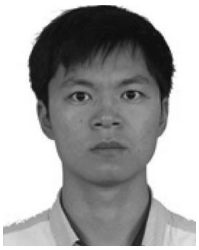

QIANGMING CAI received the Ph.D. degree in electromagnetic field and microwave technology from the University of Electronic Science and Technology. He has long been involved in computational electromagnetics and its engineering applications, electromagnetic dispersion and radiation, antenna principles and technologies, and electromagnetic compatibility.